Effects of unidirectional tensile stresses on punching shear strength of RC slabs

Pablo G. Fernández, Antonio Marí, Eva Oller, Magí Domingo

Civil and Environmental Engineering Department,
Universitat Politècnica de Catalunya,
31 Jordi Girona street, Barcelona (08034), Spain

Abstract

RC slabs can be subjected to transverse loads and in-plane tensile forces simultaneously, as it occurs in top slabs of continuous box girder bridges at intermediate supports, or in floor slabs supported on columns, due to skew in-plane compressions or imposed deformations as shrinkage. Tensile forces can reduce the punching capacity of the slabs, however, few studies have been carried out to quantify this effect. An experimental, numerical and theoretical investigation has been carried out, in which 5 1.65x1.65x0.12 m slabs have been tested under a point load and different degrees of unidirectional tensile force. Numerical predictions were made with FEA software ABAQUS and, from the theoretical point of view, the Compression Chord Capacity Model (CCCM) was extended to take into account the effect of in-plane tensile forces in the punching strength of the slabs. The experimental results showed that the ultimate punching load decreases linearly with the applied tensile force, and if that tensile force cracks the slabs, such reduction is higher. Results obtained with FEA and CCCM are in agreement with the observations made at the laboratory.

1 Introduction

The phenomenon of punching-shear has been extensively studied over the years, both theoretically and experimentally, but as far as the authors are aware, few studies have been carried out regarding punching-shear when there are tensile forces in the mid-plane of the slab [1]-[4]. Punching shear provisions included in the most frequently used design codes contemplate the effect of in-plane normal stresses in a different way. Model Code 2010 [5] formulation includes the load-rotation curves of the cross-section of the slabs, which are affected by in-plane normal stresses. ACI 318-14 [6] does not consider the effect of in-plane forces on the punching strength. However, ACI 349-06 [7] has a particular expression for the case of concrete slabs subjected to in-plane tensile stresses. Finally, EC-2 [8] includes the effect of axial stresses on punching shear by including the term $k_1 \cdot \sigma_{cp}$, but it does not differentiate between tension and compression, despite the response of concrete in one case or in the other is radically different.

RC slabs subjected to the simultaneous action of transverse concentrated loads and in-plane tensile forces can be found in continuous box girder bridges, at intermediate supports, where tensile stresses arise in top slab as result of hogging bending moments and may act together with a heavy vehicle load. Another common situation where this phenomenon takes place is on floor slabs supported on columns and subjected to a horizontal load, due to wind or earth pressure, on one of their sides. Skew compressions going from that side to the restraining columns of the opposite side may generate tensile stresses in the perpendicular direction, as can be seen in Fig. 1.

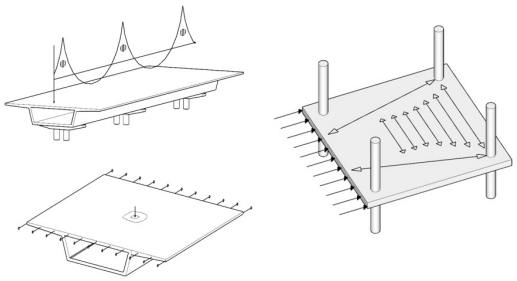

Fig. 1 Common situations where in-plane tensile stresses and a concentrate load may act together.

In this context, an experimental campaign has been carried out at the Laboratory of Technology of Structures and Materials of the Universitat Politècnica de Catalunya (UPC). The main objective of this program was to identify and quantify the effect of in plane tensile forces on the punching-shear strength of reinforced concrete slabs. On the other hand, it is intended to provide experimental results to contribute to extend the mechanically-based punching-shear resistance model "Compression Chord Capacity Model" (CCCM) [9], developed by some of the authors, to the case of in-plane tension.

From the 5 specimens tested, one was a control slab without in-plane forces (slab A0), whilst the other 4 slabs were subjected to different levels of tensile force. This article presents some results of the experimental campaign, such as load-displacement curves, crack patterns, and the decrement of the punching strength due to the tensile force applied. Experimental results have been compared with those obtained with the numerical simulations and the CCCM mechanical model.

2 Experimental campaign

2.1 Test specimens

A total of 5 slabs of 1650 x 1650 x 120 mm were cast at the laboratory. The dimensions of the slabs tested in the context of this experimental campaign are based on the punching-shear tests performed in [10]. The slabs were supported on 8 points placed at the vertices of a regular octagon, equidistant 765 mm from the point load's vertical axis, applied on its center.

The specimens were subjected to tension in their plane, in only one direction, through 10 post-tensioning bars 25 mm in diameter and 600 mm in length, partially embedded in two opposite faces (5 bars on each side) (see Fig. 2). These bars were connected to the tensioning system to apply the tensile force to the slab. The value of the external tension applied during test is measured in relation to the tensile force producing the cracking of the slab's cross section or $T_{cr} = A_c \cdot f_{ct}$, with A_c being the composite concrete and steel area of the cross section and f_{ct} the tensile concrete strength.

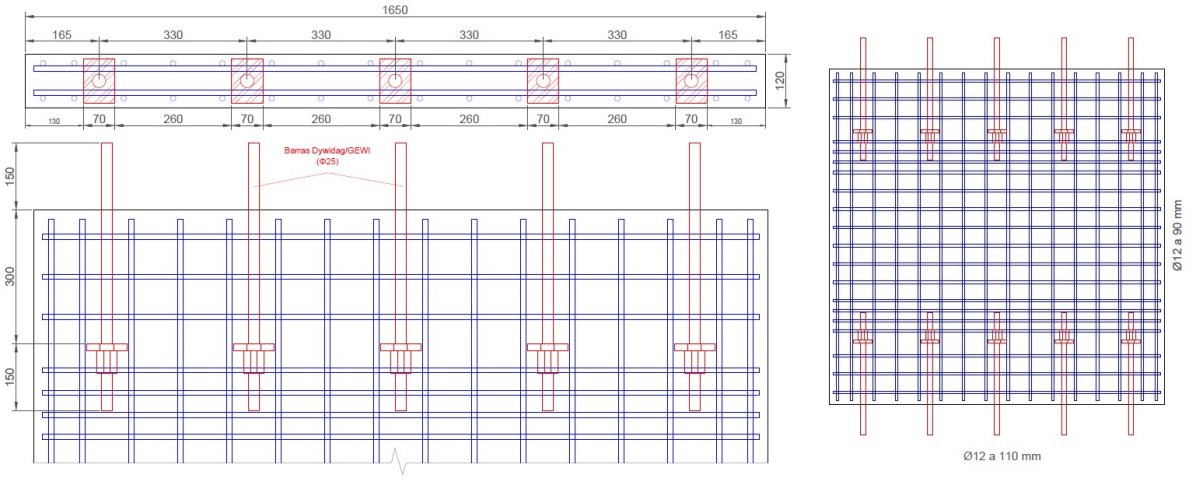

Fig. 2 Position of the post-tensioning bars inside the specimens.

The slabs were reinforced with two steel meshes arranged on the upper and lower faces. The tensile reinforcement ratio and effective depth of each slab are shown in Table 1. The punching load was transmitted to the slabs through a 145 x 145 x 30 mm steel plate located on its center. Due to the configuration of the experiment, all the slabs were tested face down with respect to their real position in a building, in which the reaction of the column goes upwards and the tensile reinforcement is arranged on the upper face.

Table 1 Reinforcement ratios and effective depths of the tension side reinforcement.

Parallel to tension			Perpendicular to tension		
Reinforcement area (mm^2)	Reinforcement ratio	Effective depth (mm)	Reinforcement area (mm^2)	Reinforcement ratio	Effective depth (mm)

1810	0.0108	99	1810	0.013	87

To characterize the materials before the control slab (A0) test, standard compression (UNE-EN 12390-3), splitting (UNE-EN 12390-6) and elastic modulus (UNE-EN 12390-13) tests were performed. The age of the concrete at that time was 160 days. The results of which are shown in Table 2.

Table 2 Mean values of material properties.

Concrete			Steel	
fc (MPa)	fct (MPa)	Ec (GPa)	fy (MPa)	Es (GPa)
37.0	3.3	29	535	215

2.2 Test set up

Four of the five tested specimens were subjected to different levels of tension, whilst the control slab was tested un-tensioned. To apply the tensile force to the slabs, an auxiliary steel structure, whose plan dimensions were 2500 x 2840 mm was built. This structure consisted of a rectangular steel frame surrounding the slab (Fig. 3)

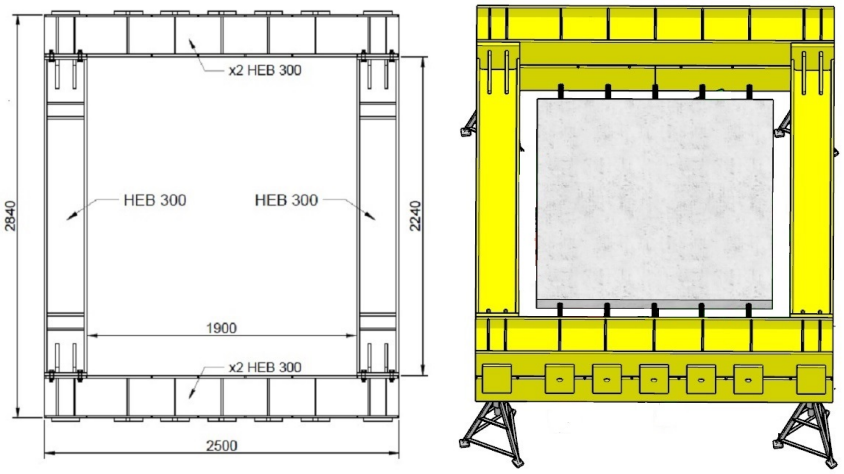

Fig. 3 Steel frame used to apply tensile force to the slabs

On one of the faces, a passive anchor for the tensioning bars was used, meanwhile bars were prestressed from the other end, with the help of hollow jacks connected to the protruding bars. The force applied to the slab was measured by a set of hollow load cells placed at both anchorages.

The steel structure was set at the appropriate height with the help of four height-adjustable supports designed for the experimental campaign and located under each of the four corners of the frame. For safety reasons, once the desired external force value was reached, the extension bars were anchored and the jacks were disconnected from them. The tensile force applied to the slabs in each test is presented in Table 3.

Table 3 Values of tensile forces applied on each test

Test #	T/T_{cr} at failure
1	0.00
2	0.44
3	0.69
4	1.02
5	1.26

To introduce the punching load, a hydraulic jack anchored in a loading frame, rigidly fixed to the floor slab, was used. Eight 120 x 120 mm load cells were placed at slab supports to measure the reactions, arranged in a circle centered with respect to the center of the loading frame. A piece of rubber was placed over each of the cells to allow free rotation in the supports. The 8 load cells were supported on 4 rigid easels arranged in such a way that the distance between the axis of two opposite supports was 1530 mm (Fig 4).

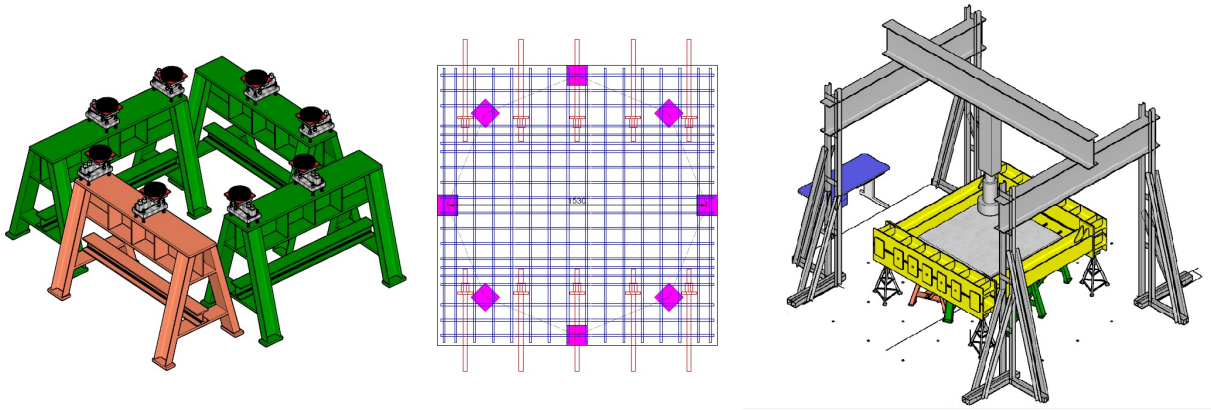

Fig. 4 Support schema of the slabs (left and center) and final positioning of all the elements under the loading frame (right)

3 Mechanical model. Extension of CCCM

3.1 Shear and punching models

The Compression Chord Capacity Model (CCCM) is a simplified shear strength mechanical model derived from a more general model called Multi-Action Shear Model (MASM), developed by A. Marí, et al. [11] and Cladera et al. [12]. It considers, as it is widely accepted, that the shear strength (V_{rd}) is the sum of: the shear resisted in the un-cracked compression head (V_c), the shear transferred across the web cracks (V_w), by aggregate interlock and residual stresses, the shear resisted by the longitudinal reinforcement, due to dowel action (V_{cl}), and the contribution of the transverse reinforcement (V_s), providing explicit expressions for each component. The CCCM model, groups the three first components into a single one, V_c, called concrete contribution.

Distributions of normal and shear stresses are assumed by combining beam and arch effects, so that the compression chord is subject to a biaxial stress state. It is considered that failure occurs when the principal stresses at one point of the compression head, at a critical section defined in [9], reach the Kupfer's biaxial failure envelope, in the compression-tension branch. To obtain the beam shear strength, equilibrium of forces and moments between the internal forces (V, M) and the stress resultants (Fig. 5) at the concrete chord (C, V_c), along the crack (V_w), at the stirrups (V_s) and at the longitudinal reinforcement (T, V_l) are taken in the portion indicated by Fig. 5. Then, relating forces with stresses and taking into account the failure criterion, the ultimate shear is obtained.

This model was extended to punching [9], considering the main differences between both phenomena, in order to incorporate them into the mechanical model. First, taking into account the shape of radial bending moment law $m_r(r)$, the position and inclination of the critical crack were formulated. Thus the position of the control perimeter was obtained. The second important effect incorporated was the multiaxial stress state in the slab compressed chord, due to tangential and vertical stresses in the vicinity of the column, enhancing the concrete capacity to resist shear stresses in the radial vertical plane. This phenomenon was is incorporated in the model by modifying the compression-tension branch of Kupfer's biaxial failure envelope, using the confined concrete strength f_{cc}, from the EC-2 [8] formulation, instead of the unconfined strength f_c, so that a higher shear stress is needed to reach failure. Again, to obtain the punching strength of the slab, the equilibrium between internal forces and stress resultants is taken in a portion of the slab enclosed by the critical perimeter and the critical section (Fig. 6).

Solving the equilibrium equations, and assuming some simplifications explained in [9], the simplified expression for the punching strength (2) is derived, where ζ is the size effect given by Eq. (3) and x/d is the relative neutral axis depth obtained assuming cracked concrete, zero tensile stresses and linear stress distribution in the compression chord.

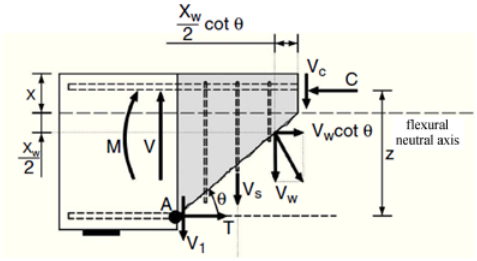

Fig. 5 Shear transfer mechanism and scheme of the equilibrium of the considered forces in the shear model.

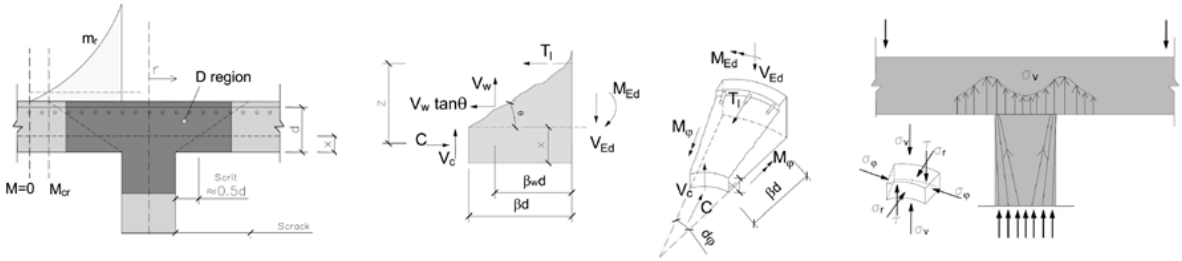

Fig. 6 Shear transfer mechanisms and scheme of the equilibrium of the considered forces in the punching model.

$$V_{rd,0} = 0.3 \cdot \zeta \left(1.125 \cdot \frac{x}{d} + 0.425\right) f_{ck}^{2/3} \cdot u_{cri} \cdot d \tag{2}$$

$$\zeta = \frac{2\left(\frac{d}{a}\right)^{0.2}}{\sqrt{1 + {}^{d}/_{100}}} \tag{3}$$

Due to the internal redundancy of the slabs, flexural reinforcement may yield before punching failure occurs, leading to a flexural-punching failure. First yielding will take place when the tangential moment reaches the lower yielding moment of the two orthogonal directions, since tangential moment per unit length is higher than the radial moment, and a redistribution of moments may take place from that point onwards. Anyhow, the punching strength can't be higher than the load that equals the radial moment to the yielding moment per unit length (Vy) at the control perimeter.

$$m_r = \frac{V}{4\pi}\left[(1+\nu)\ln\frac{r_0}{r_{cri}}\right] \approx \frac{V}{2\pi} = m_y = \rho f_y d^2\left(1 - \frac{\rho f_y}{2f_c}\right) \tag{4}$$

$$V_{rd,0} \leq V_Y \approx 2\pi m_y \approx 2\pi f_y d^2\left(1 - \frac{\rho f_y}{2f_c}\right) \tag{5}$$

In equation (4) it has been assumed, for the sake of simplicity, a mean value of $r_0/r_{cri} = 5$ and a Poisson's ratio for cracked concrete $\nu = 0.3$

3.2 Extension of CCCM-punching to in plane tensile forces

Since CCCM is a mechanical model, the effects of the tensile force were accounted for in two ways: by including it into the equilibrium equations, and using a previously derived reduction of the neutral axis depth due to the presence of that tensile force [13]. Then, a new simplified expression was derived (6). For the particular case of unidirectional tension, where half of the perimeter is subjected to tension and the other half remains un-tensioned, shear strength, is given by Eq. (7).

$$V_{rd,T} = \zeta\left[(1.125 - 0.85)\frac{x}{d} + 0.425\right] f_{ck}^{2/3} \cdot u_{cri} \cdot d \tag{6}$$

$$V_{rd,total} = \frac{V_{rd,0}}{2} + \frac{V_{rd,T}}{2} = \left(V_{rd,0} - 0.425 \cdot \zeta \cdot \frac{T}{T_{cr}} \cdot \frac{x}{d}\right) f_{ck}^{2/3} \cdot u_{cri} \cdot d \tag{7}$$

Where T_{cr} is the force producing cracking in the RC slab due to pure tension. For values of $T>T_{cr}$, no contribution of the concrete to resist tension is considered, being resisted only by the reinforcement. For this cases, an effective tensile strength of steel $f_y^* = f_y - T/A_s$ is adopted, and used in Eq. (5). This reduction provokes that V_y, the punching strength associated to reinforcement yielding, becomes dominant, diminishing even more the strength and stiffness of the slab, as can be seen in section 5.

4 Numerical simulations

In addition to the experimental campaign, a numerical model was developed to contrast the obtained results at the laboratory and with the mechanical model CCCM. Simulations were carried out with Simulia Abaqus software, using the Abaqus/Explicit package [14].

4.1 Model generation

Taking account the existing double symmetry, both in geometry and loading, only a quarter of each slab was simulated, considering the corresponding boundary conditions in each symmetry plane. For concrete, cubic elements of 8 nodes (C3D8R) were used while for reinforcing bars, linear beam elements of 2 nodes (B31) were used [15]. The reinforcing bars were considered perfectly bonded to the concrete. The size chosen for the elements were 20 mm, so that 6 elements were arranged along the 120 mm of the slab's thickness. The slab supports were simulated by means of non-linear springs (SPRING A), with a very high stiffness in compression and practically zero stiffness in tension, thus allowing the partial lifting of the slabs. The introduction of the tensile force was simulated by applying the loads directly to the nodes located in the area of the anchor plates of the post-tensioning bars, whilst for the punching load, a displacement was imposed on the nodes located on the upper face of the slab, under the surface occupied by the load plate.

4.2 Materials

The Concrete Damaged Plasticity model [16] was chosen to simulate the behavior of concrete, which requires the definition of the uniaxial constitutive equations in compression and tension, in addition to the definition of a yielding surface. To define the yielding surface default values were used except for the dilation angle ($\psi = 37.5º$) and $K = 0.8$. For compression, the Hognestad parabolic constitutive equation was selected, with a linear behavior up to 40% of f_c (σ_{c0}). For the tensile behavior the model proposed in section 5.1.8.2 of the Model Code 2010 [7] has been used. To define the elastic response, only the modulus of elasticity (E_c) and the Poisson ratio (ν) are needed. E_c was obtained in the corresponding characterization test (see Table 2), while for ν, as Abaqus/Explicit considers it a fixed value throughout the whole simulation process, including post-cracking regime, $\nu = 0$ was used [15].

5 Results

In this section, experimental, numerical and theoretical results are compared, focusing on the relative decrement of the punching strength to the tensile force applied. The numerical model was adjusted to fit the experimental results obtained in the control test. Once it was verified, simulations were performed for several values of T/Tcr, up to a maximum of T/Tcr = 1.5, in order to obtain a more complete behavior curve. Figure 6 shows the comparison between the load-deflection curves obtained experimentally and numerically for three of the test carried out at the laboratory. As can be seen, quite accurate results were obtained in terms of the ultimate load.

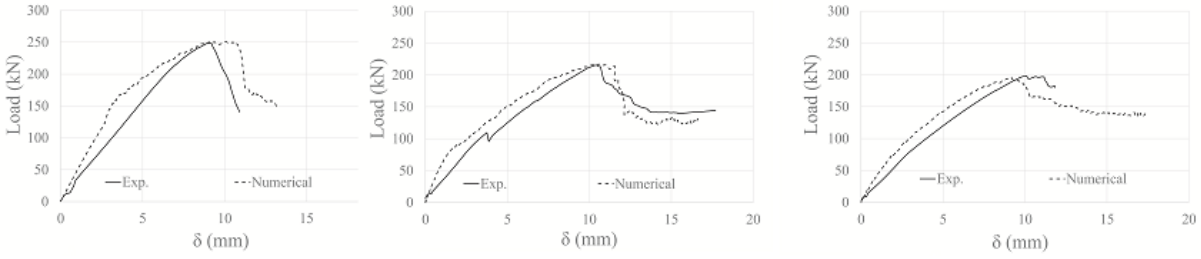

Fig. 6 Comparison between load-deflection curves obtained with the numerical model and experimentally for T = 0 (left), $T/T_{cr} = 0.69$ (center) and $T/T_{cr} = 1.02$ (right)

Figure 7 shows how the punching strength decreases as T/T_{cr} increases, and that this decrement is even bigger for values of $T/T_{cr} > 1$. A very good correlation between experimental, numerical and analytical models is observed as summarized in table 4.

Table 4 Relative decrement of the punching strength to the tensile force obtained with each method

Test #	T/T_{cr} at failure	$P_{u,0}/P_u$ *(Experimental)* ($P_{u,0}$=249.1 kN)	$P_{u,0}/P_u$ *(CCCM)* ($P_{u,0}$=235.9 kN)	$P_{u,0}/P_u$ *(numerical)* ($P_{u,0}$=250.3 kN)
1	0.00	1	1	1
2	0.44	0.91	0.92	0.93
3	0.69	0.86	0.87	0.88
4	1.02	0.79	0.81	0.81
5	1.26	0.72	0.72	0.73

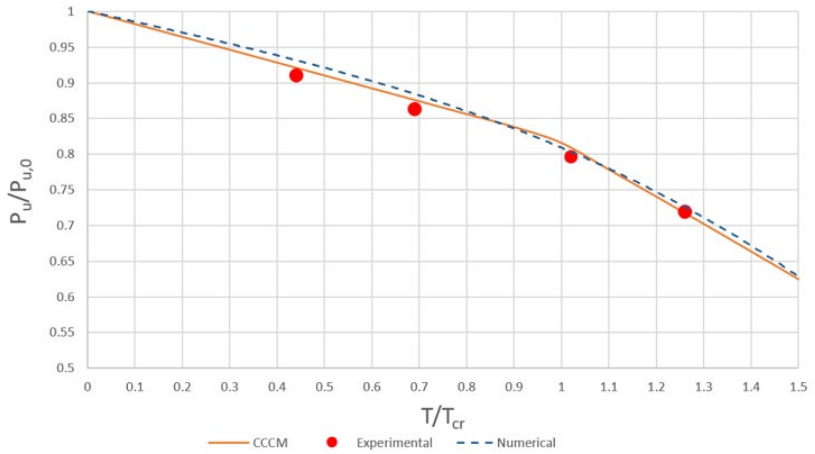

Fig. 7 Comparison of the relative decrement of the punching strength to the tensile force obtained numerically, theoretically and at the laboratory.

Finally, different crack patterns obtained numerically are shown in Fig. 8. As can be seen, the radial pattern obtained for T = 0 evolves into an orthogonal pattern for high values of T/T_{cr}

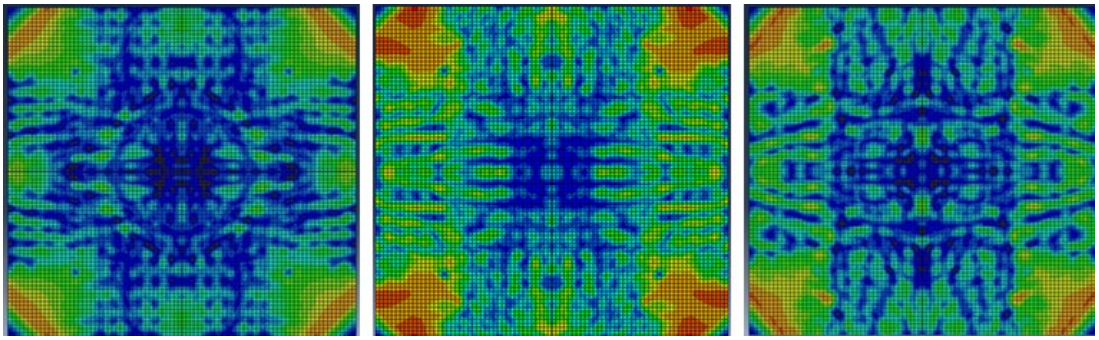

Fig. 8 Crack patterns (in blue) for T = 0 (left), $T/T_{cr} = 0.69$ (center) and $T/T_{cr} = 1.26$ (right). (Tensile force applied in horizontal direction in the pictures)

6 Conclusions

Based on the observations made during the experimental campaign and the results presented in this article, the following conclusions can be drawn:

- The decrease in the punching-shear strength can be well characterized by a bilinear function of the applied tensile force "T". The first branch arrives up to a certain value "T_{cr}", after which a higher reduction of the punching strength is observed.
- The maximum value of the reduction produced by the presence of a tensile force, for the tests carried out, was 28% with respect to the reference slab, for a load $T = 1.26\ T_{cr}$. For the tensile value $T = T_{cr}$, the punching load reduction was approximately 20%
- Both the numerical model developed and the extended theoretical model CCCM have been able to accurately reproduce the results of an experimental campaign carried out by the authors. The experimentally observed behaviour has been captured both qualitatively and quantitatively, with an average error on the prediction of the ultimate load of 5%

Acknowledgements

This work has been carried out within the framework of research project BIA-2015-64672-C4-1-R, financed by the Ministry of Economy and Competitiveness (MINECO) of Spain. The authors want o deeply thank the personnel of the Structural Technology Laboratory of the Polytechnic University of Catalonia and Master student Laura Beltrán who collaborated in the execution of the tests.

References

[1] Abrams, J.H. The Punching Shear Strength of Pre-cracked Reinforced Concrete in Biaxial Tension", M.S. Thesis Cornel University, May 1979.
[2] Jau, W.C, White R.N, Gergely P. Behavior of reinforced concrete slabs subjected to combined punching and biaxial tension. Report for U.S. Nuclear Regulatory Commission, 1982.
[3] Regan, P.E. Punching shear in prestressed concrete slab bridges. Engineering Structures Research Group, Polytechnic of central London, 1983.
[4] Bui T.T, Nana W.S.A, Abouri S, Liman A, Tedoldi B, Roure T. Influence of uniaxial tension and compression on shear strength of concrete slabs without shear reinforcement under concentrated loads. Construction and Building Materials 2017:147;86-101
[5] Fédération international du Béton. Fib Model Code for Concrete Structures 2010 xol. 1. Lausanne: Ernst & Sohn; 2013
[6] ACI 318-14. Building code requirements for structural concrete and commentary. American Concrete Institute, 2014.
[7] ACI 349-06. Code Requirements for Nuclear Safety Concrete Structures. American Concrete Institute, 2007.
[8] European Committee for Standardization. Eurocode 2: design of concrete structures: Part 1: general rules and rules for buildings. Brussels: European Comittee for Standarization; 2002.
[9] Marí A, Cladera A, Oller E, Bairán JM. A punching shear mechanical model for reinforced concrete flat slabs with and without shear reinforcement. Eng. Struct. 2018:166;413-26
[10] Polak MA. SP-232: Punching shear in reinforced concrete slabs. Am Concrete Institute, Spec Publ, vol. 232; 2005. P.302. http://dx.doi.org/10.14359/14960.
[11] Marí, A.; Bairán, J.; Cladera, A.; Oller, E.; Ribas, C. "Shear-flexural strength mechanical model for the design and assessment of RC beams". Struct. And Infr. (2014) Eng. 11:1399–1419,
[12] Cladera, A., Marí, A., Bairán, JM. Oller, E., Duarte, N. (2016) "The compression chord capacity model for the shear design and assessment of reinforced and prestressed concrete beams" Structural Concrete (fib), Wiley, 18-2, pp1017-1032, ISSN 1464-4177
[13] Fernández, P.G.; Marí, A.; Oller, E.; Domingo, M., Effects of tensile stresses on punching shear strength of RC slabs.(2019). 5th Int'l. Conf. Mech. Models Struct. Eng. CMMoST, Alicante, Spain
[14] Abaqus Analysis user's manual 6.14, Dassault Systems Simulia Corp., Providence, RI, USA; 2014
[15] Genikomsou A, Polak MA. A Finite Element analysis of punching shear of concrete slabs using damaged plasticity model in ABAQUS. Eng. Structures 2015:98;38-48
[16] Lubliner J, Oliver J, Oller S, Oñate E. A plastic-damage model for concrete. Int J Solids Struct 1988;25(3):299-326